2020 16th IEEE International Conference on Automation Science and Engineering (CASE)
August 20-21, 2020, Online Zoom Meeting

Design and closed loop control of a 3D printed soft actuator

Qinglei Ji[1,2], Xiran Zhang[1], Mo Chen[2], Xi Vincent Wang[2], Lihui Wang[2] and Lei Feng[1]

Abstract— **Soft robots, made of soft materials such as dielectric elastomer or shape memory polymers, have received tremendous attentions due to its dexterousness, flexibility and safety compared with rigid robots. However, wider application of soft robots is limited due to their complex fabrication process and poor controllability. Here, we introduce a closed loop controlled soft actuator that is fully 3D printed with flexible material. The structure of the soft actuator is optimized with Finite Element Method (FEM) to acquire shortest fabrication time and highest deformation for same stimulus input. A desktop Fused Deposition Modeling (FDM) 3D printer is used for low-cost fabrication of such actuators. A webcamera is used for the image feedback which offers the real time shape monitoring of the soft actuator. An output feedback Proportional Integral Derivative (PID) controller with lowpass filter is developed with pole placement design method based on a data-driven model of the 3D printed soft actuator. The controller is implemented to regulate the input air pressure to ensure a fast-response, precise and robust shape changing for any work environments.**

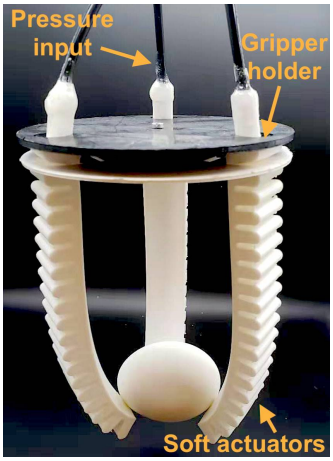

Fig. 1: 3D printed soft gripper.

I. INTRODUCTION

Soft actuators are made from highly compliant materials and are employed by soft robots. Compared with their counterparts, rigid robots, that use hinges, gears or other transmission devices to transmit force and movements to further locations, soft robots are better at continuous movements, smooth motions, safe interactions and are featured with equal force distribution [1], [2]. Subsystems such as different sensors, actuators, and controllers are also integrated with the soft body to increase the dexterousness and controllability of soft robots. These features make soft robots an ideal candidate for applications that need complex actuation and reduced energy consumption or environments that humans are included which have high safety requirements. As a result, soft robots are catching more and more attentions in the academic and industry field.

Following different stimulus methods, soft actuators can be classified into various groups such as pressure-driven, thermo-driven, electro-driven, light-driven, liquid-driven and magneto-driven etc [3]. Accordingly, different materials like flexible polymers [4], thermoresponsive polymers [5], Electroactive Polymers (EAP) [6], light sensitive materials [7], hydrogels [8] and magnetic particles [9] are either used as the matrix or the fillers for construction of stimulus responsive soft actuators. Most soft actuators are fabricated in multi-steps [3] with technologies such as moulding [10] and mask lithography [11]. However, these technologies normally require many devices and multiple preparation processes. Furthermore, mature operation skills are necessary for a consistent and reliable prototype. These disadvantages limite applications of soft robots in the market.

3D printing (3DP) is a novel manufacturing technology featured with depositing material layer by layer and often used for fast prototyping of novel design. 3DP shows great advantage in terms of free form of design, easiness of operation, material-saving and cost-efficiency. 3DP tends to be a good choice for the preparation of soft robots. Different 3DP technologies have been used for fabricating diverse soft actuators to accomplish different tasks. Composite hydrogel architectures are 3D printed with Direct Ink Writing (DIW) technology to form anisotropic swelling behaviour induced by the alignment of cellulose fibrils that mimics the cellulose fibrils distribution within plant cell walls [12]. Magnetic particles and elastic polymer mixtures are printed with a refitted DIW nozzle that is able to perform local programming of the magnetic particles directions such that the fast-transforming actuations are enabled [9]. Thermoplastic polyurethane (TPU) filaments are used for Fused Deposition Modeling (FDM) printing of a soft pneumatic gripper that can endure heavy load [4]. UV curable elastomers are 3D printed with Digital Light Processing (DLP) process for fabricating pneumatic and highly stretchable soft actuators with sub-micrometer precision [13]. Hydrophilic polymer that expands tremendously when encounters water is printed with multi-material PolyJet (PJ) printing technology. PJ

*The research is financially supported by Swedish Research Council (Vetenskapsrådet) with the project 'Closed-Loop 4D Printing with High Precision', number 2017-04550 and KTH XPRES. (Corresponding author: Lei Feng. e-mail:lfeng@kth.se)

[1]Department of Machine Design, KTH Royal Institute of Technology, Stockholm 10044, Sweden

[2]Department of Production Engineering, KTH Royal Institute of Technology, Stockholm 10044, Sweden

printing enables rigid material and such hydrophilic polymer to be printed simultaneously with designed and differentiated distributions so that the 3D printed material reveals different local morphings [14]. Shape memory alloys (SMA) are embedded during PJ printing process to excite bending actuation of the whole printed body [15]. The considerations of embedding components into parts during the 3DP process brings more possibilities for 3D printed soft actuation.

Most of the currently 3D printed soft actuators, however, are designed and created without considering their actuation precision and controllability. Recently, there is an emerging tendency of integrating sensors and controllers during the 3DP process so that the actuation of the 3D printed soft robots can be monitored, analyzed and regulated. Santina et al. [16] proposed a closed loop dynamic controller enabling a continuous soft pneumatic robot to be capable of dynamically tracking desired curvatures and moving in Cartesian space. A motion tracking system provides real-time measurements of marked points on the soft actuator as the feedback signal. Bajo and Simaan [17] complete a framework for hybrid motion/force control of multi-backbone continuum robots with force feedback provided by a multi-axis force sensor. Furthermore, scholars are combining data-driven/Machine Learning (ML) models and dynamic controllers to make the soft robots actuate in a faster, more precise, more time-efficient and energy-efficient manner [18], [19].

Here, we report a 3D printed soft pneumatic actuator that is closed loop controlled using an output feedback Proportional Integral Derivative (PID) controller with lowpass filter. Influences of the key dimensions that determine the structure of the soft actuator are analyzed and studied with Finite Element Method (FEM). A group of parameters that enable largest deformation under the same pressure input are selected for fabricating the soft actuator. The soft actuator is 3D printed with a desktop low-cost 3D printer. Images captured with a webcamera are analyzed in real time to acquire the instant bending angle of the soft actuator. An output feedback PID controller with lowpass filter is acquired based on a data-driven model established with the experiment data to regulate the pressure input accordingly so that the actuation shape is quickly and robustly altered to target position with high precision for different working conditions. The work demonstrates a cost effective method of producing closed loop controlled soft actuators.

The rest of this paper is organized as follows. Section II.A describes the design and optimization of the actuator structure with FEM. Section II.B elaborates the fabrication of the soft actuator with 3DP technology. Section II.C studies the modelling of the fabricated soft actuator under different air pressure stimulus. Section II.D and Section II.E introduce the design and implementation of an output feedback PID controller with lowpass filter for the closed loop shape control of the actuator. The control results are analysed and compared with previous study. Finally, this paper is concluded and some further research directions are proposed in Section III.

II. Design and Experiments of the Soft Actuator

A. Optimization of soft actuator design

The actuator studied in the article is a bellows-type actuator [4], [20], [21] which generates deformation by unfolding the bellows. Compared with other types of soft actuators, bellows-type actuators exhibit larger deformation for the same input pressures, which proves their energy efficiency from one aspect. The bellows structure also minimizes the overall stress on the soft actuator, which prolongs the life period and improves the robustness of such actuator. To further improve the performance of the actuator in this study, FEM method through Abaqus (ABAQUS Inc.) is used to optimize the key parameters to achieve largest deformation under the same input pressure. As shown in Fig. 2, the parameters such as the number of air chambers N for a certain length of actuator, thickness of the chamber walls t_{wall} and the height of the vent h_{vent} that enables air pressure to transmit to every chamber, configure the local shape for a actuator with a fixed overall size, which is $L \times W \times H = 150\ mm \times 25\ mm \times 15\ mm$ in this study. An Ogden model is used as the constitutive model, similar to what Yap et al has established in their study [4] and same model parameters are used.

Different configurations of the aforementioned parameters are modeled with FEM and stimulated with a constant pressure input of $1bar$. To study the influence of the three parameters, we perform the following tests. Firstly, the number of chambers is varied from 9 to 19 with a fixed chamber wall thickness of $1.1\ mm$ and a fixed height of vent of $0.3\ mm$. Secondly, the wall thickness is varied from $1.1\ mm$ to $1.8\ mm$ with a fixed number of chambers of 19 and a fixed height of vent of $0.3\ mm$. Finally, the height of vent is varied from $0.3\ mm$ to $0.8\ mm$ with a fixed number of chambers of 19 and a fixed chamber wall thickness of $1.1\ mm$. The

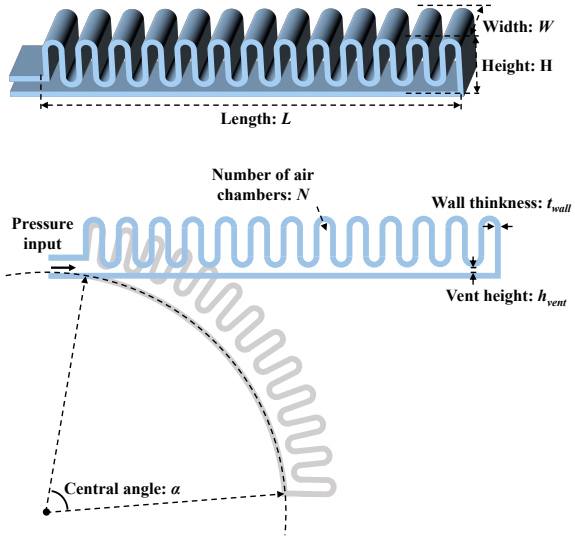

Fig. 2: Influences of the key parameters of the soft actuator on the shape deformation.

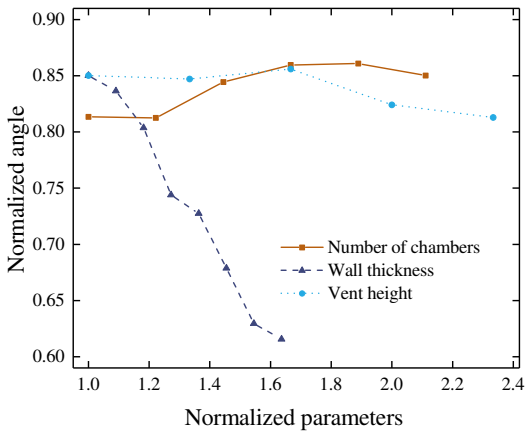

Fig. 3: Key dimensions of the bellows-type actuator.

bending of the soft actuator is expressed with the central angle of the arc that is formed by the bent actuator as shown in Fig. 2. Bigger bending degrees cause larger central angle and vice versa. The varying parameters are all normalized with the minimum value among the parameters respectively. For example, the number of chambers is normalized with the minimum used number of chambers 9. The central angles are normalized with $180°$ for easier comparison of the effects of the different parameters. Fig. 3 shows the impact of the three groups of parameters on the deformation of the soft actuator. The bending becomes larger while increasing the number of chambers. However this tendency becomes less obvious for larger amount of chambers. Further increasing the number of chambers adds the fabrication complexity and material consumption. The vent height has slight and irregular impact on the deformation. Smaller vent height roughly causes larger deformation. However, considering the 3D printing capability, the value of vent height cannot be too small to avoid contact between the printed walls. The wall thickness shows greatest influence on the deformation. Increasing the wall thickness significantly decreases the bending degree. Thus, a thinner wall is desired. However, too thin walls result in the risk of leakage of air pressure, making the actuation unstable and unpredictable. on the basis of previous discussions and 3D printing tests, the final parameter is chosen as $N = 19, t_{wall} = 1.3\ mm$ and $h_{vent} = 0.3\ mm$ to ensure a credible fabrication and reliable functioning of the 3D printed actuator. More details on the selection of these parameters are presented in our earlier study [22].

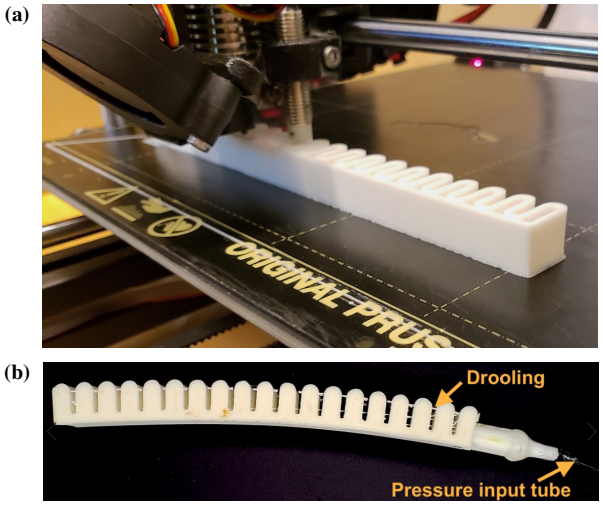

Fig. 4: Fabrication process of the soft actuator. (**a**) 3D printing with an FDM 3D printer. (**b**) Soft actuator connected with the pressure input tube.

B. 3DP of the soft actuator

The soft actuator is 3D printed with a Prusa i3 MK3 FDM 3D Printer (Prusa Research a.s.) which is equiped with a direct-drive extruder as shown in Fig. 4(a), making it good at printing flexible materials by reducing the risk of buckling of the soft material [4]. The print augments along the width direction with an infill percentage of 100% and no support material. Detailed 3D printing parameters can be found in Table I. After being printed, the predesigned connector for intake air pressure is connected with a $4\ mm$ outer diameter Polytetrafluoroethylene (PTFE) tube for pressure supply and sealed with Epoxy adhesive (Loctite EA 3430) as shown in Fig. 4(b). Note that small material drooling is found between the bellows of the soft actuator. The drooling is caused by the residual pressure in the heating extruder and the material still extrudes out from the extrusion head while the print head

TABLE I: 3D printing parameters

Parameters	Features
Layer height (mm)	0.1
First layer height (mm)	0.2
Fill	
Fill density $(\%)$	100
Overlap $(\%)$	45
Horizontal shells	
Top	7
Bottom	5
Brim	No
Support	
Support on build plate only	
Speed	
Print speed (mms^{-1})	20
First layer speed (mms^{-1})	10
Temperature	
Extruder temperature $(°C)$	240
Bed temperature $(°C)$	60
Filament	
Diameter (mm)	1.75
Extrusion multiplier	1.6
Machine	
Nozzle size (mm)	0.4

switches its position. This phenomenon is found to be more obvious for flexible materials compared with rigid materials such as polylactic acid (PLA).

C. Model identification

With the 3D printed prototype, a series of pressure stimulus tests are performed to acquire the response characteristics of the soft actuator for the future controller design. Pressure inputs P varying from $0.6\ bar$ to $1.6\ bar$ are applied and the changing of the central angle of the soft actuator is recorded versus time. As shown in Fig. 5(a), the final steady angle shows good linear relation to the input pressure, which reveals the good linearity of the system response. The response angles recorded in different stimulus tests are then normalized to acquire the DC gains using the pressure inputs respectively as shown in Fig. 5(b). Different groups of response data are then averaged and fitted to estimate the transfer function of the model using $tfest$ command in Matlab. Models of different orders are used to fit the response data as shown in Table II. Root Mean Square Error (RMSE) between the predicted data of the model and the real value

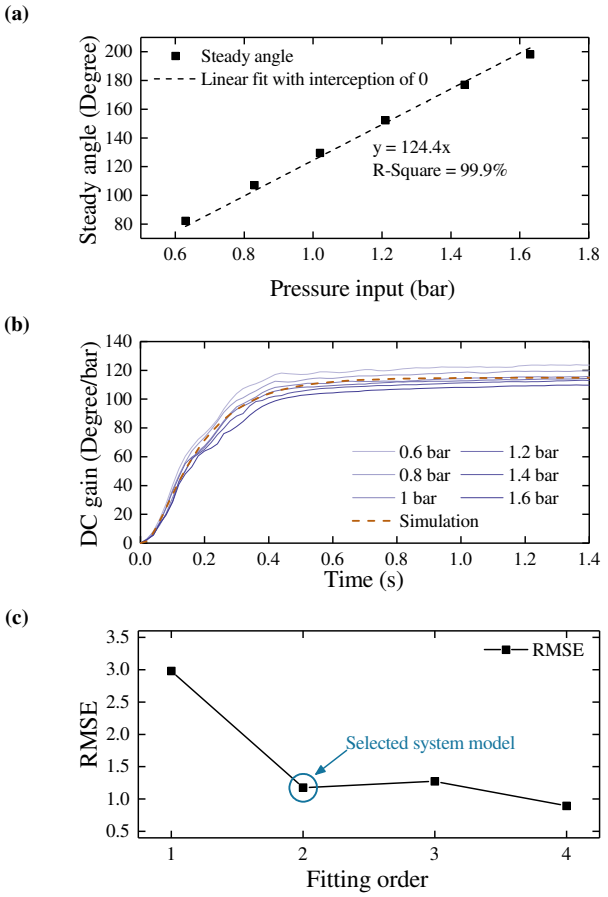

Fig. 5: Model selection. (**a**) Steady response angle versus different pressure inputs. (**b**) Response of the soft actuator under different pressure inputs. (**c**) RMSE between the experiment data and the models of different orders.

TABLE II: fitting results

Order	System $\frac{\alpha(z)}{P(z)}$	RSME
1	$\frac{11.82}{z-0.90}$	2.98
2	$\frac{1.30z+3.90}{z^2-1.52z+0.56}$	1.18
3	$\frac{1.44z^2+3.35z-3.13}{z^3-2.17z^2+1.55z-0.36}$	1.27
4	$\frac{-0.12z^3+7.60z^2-13.76z^1+6.48}{z^4-3.17z^3+3.70z^2-1.86z^1+0.33}$	0.89

are used to evaluate the goodness of fitting. Fig. 5(c) shows that the second order transfer function is found to offer a much higher matching degree with small RMSE than first order model. Higher orders of the models do not significantly reduce the errors. Thus the second order model is selected to describe the soft actuator system considering the simplicity for further calculations. The discrete transfer function of the model is expressed in Equation (1):

$$G_p(z) = \frac{\alpha(z)}{P(z)} = \frac{1.30z + 3.90}{z^2 - 1.52z + 0.56} \tag{1}$$

The sampling time is $T_s = 0.02\ s$.

D. Closed loop shape control and controller design

With the fitted response model, an output feedback PID controller with lowpass filter for shape control is applied to realize the automated and precise shape morphing of the soft actuator. The control structure is illustrated in Fig. 6. The controller compares the difference between the position reference and the actual shape position that is acquired by analysing the real time pictures captured by a Logitech C270 HD Webcamera. The controller then calculates a suitable pressure value for stimulating the soft actuator and sends the relevant electric voltage level signal to a proportional pressure regulator (Festo VEAB-L-26-D9-Q4-V1-1R1) that is connected to a pressure source of 6 $bars$ and the soft actuator. According to the voltage level, the pressure regulator alters its pressure output accordingly and supplies it to the soft actuator. The output feedback control law [23] can be expressed as Equation (2):

$$P_r(z) = G_{ff}r - G_c\alpha \tag{2}$$

where $P_r(z)$ is the pressure reference sent to the pressure regulator. The pressure regulator is assumed to be an ideal regulator and provides pressure output $P(z)$ equal to the pressure reference $P_r(z)$ with no delay. The output feedback controller selects G_c to reject disturbances in the pressure input and the angle output, and selects G_{ff} to have desired response to r. Pole placement method is applied here to acquire the appropriate controller parameters. The control structure of G_c for the output feedback PID controller with lowpass filter can be expressed as Equation (3):

$$G_c = \frac{S(z)}{R(z)} = \frac{s_2z^2 + s_1z + s_0}{(z-1)(z+r_0)} \tag{3}$$

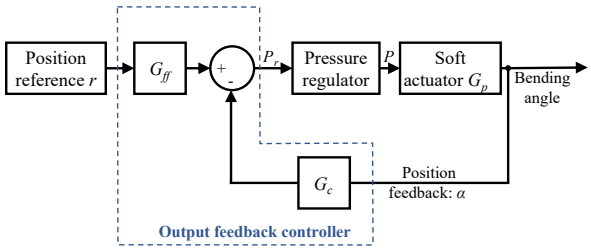

Fig. 6: Closed loop control structure.

where s_2, s_1, s_0 and r_0 are the parameters defining the controller and need to be calculated with assumed poles. The closed loop specifications define the closed loop polynomial $A_{cl}(z) = A_m(z)A_0(z)$, where A_m has the same order as $G_p(z)$ and can be expressed as $A_m = (z - w_1)(z - w_2)$. With four parameters to be decided, A_0 should also be a second order function and can be expressed as $A_0 = (z - w_3)(z - w_4)$. w_1, w_2, w_3 and w_4 are the pole positions that determine the characteristics of the closed loop system and need to be pre-defined with aid of the system model and then fine tuned with experimental methods. The Diophantine equation [23] can be expressed as Equation (4):

$$P(z)R(z) + \alpha(z)S(z) = (z - w_1)(z - w_2)(z - w_3)(z - w_4) \tag{4}$$

s_2, s_1, s_0 and r_0 are computed by solving the Diophantine equations. The feed forward part G_{ff} can be expressed as Equation (5):

$$G_{ff} = \frac{T(z)}{R(z)} \tag{5}$$

where $T(z) = t_0 A_0(z)$ and t_0 is defined as $t_0 = \frac{A_m(1)}{\alpha(1)}$ such that the DC gain from the reference to the output is 1.

E. Controller implementation and analysis

With the designed controller and 3D printed soft actuator, a closed loop shape control is performed experimentally. Fig. 7(a) shows the schematic of the experimental setup. The webcamera is located on top of the soft actuator for monitoring with a frame rate of 30 frames per second (fps) as shown in Fig. 7(b). The pictures are then analysed with a Raspberry Pi 4. Fig. 7(c) shows the view of the webcamera. Three black mark points are drew along the length of the soft actuator to provide the bending edges for further image processing.

The requirement of the closed loop control includes

- Rise time should be as short as possible to enable fast actuation.
- No overshot is permitted to avoid excessive deformation than the reference.
- Oscillation should be less than 1% of the reference for a steady shape maintenance.

To meet the requirements, multiple groups of pole positions are tested experimentally and a best selection of pole values are set as: $w_1 = w_2 = 0.7711$ and $w_3 = w_4 = 0.9012$. In our earlier work, an error feedback PI controller was

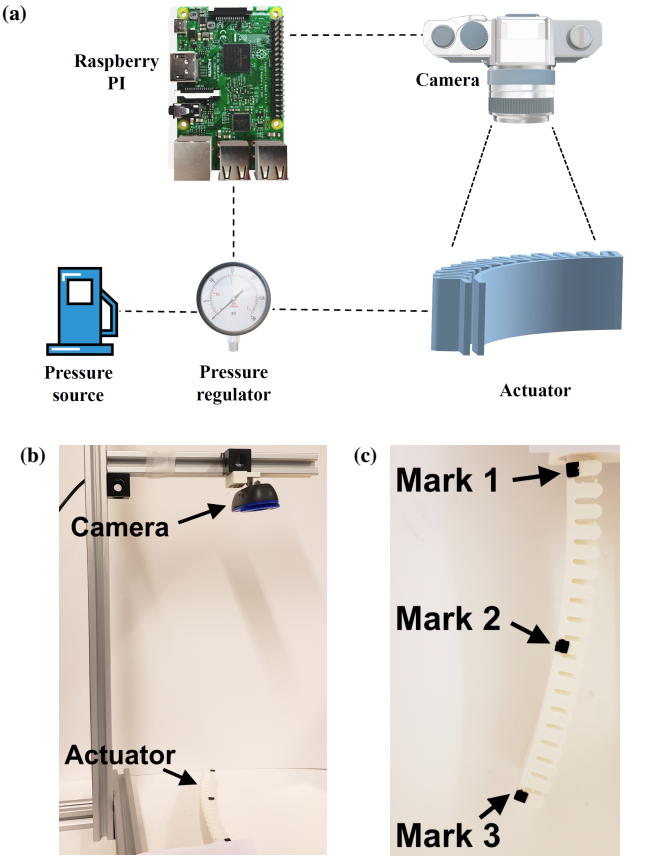

Fig. 7: Experiment setup of closed loop control set-up for the soft actuator. (**a**) Schematic of the experimental setup. (**b**) A camera is mounted above the soft actuator. (**c**) The view captured by the webcamera.

applied to perform the shape control [22]. The PI controller was fine tuned and the controller parameters were set as $P = 0.0074$ and $I = 0.0455$ to provide satisfying control results. The results are plotted together with the control results of the aforementioned output feedback controller with lowpass filter for a comparison as shown in Fig. 8. Examples of controlled angle changes from $30°$ to $50°$, $70°$ and $90°$ are plotted. The dash dotted orange line shows the position reference change from $30°$ to $50°$ at the moment 0 s. The central angle of the soft robot also starts to vary from its original position to $50°$ as shown by the solid purple line in the same figure. The dashed purple line shows the simulation angle change and the light blue line shows the variation of the input pressure with its values marked on the right axis. The key features of the two control results are concluded in Table III. For the three control tests, both controllers achieve stable shape changes with static error less than 1% of the desired deformation for each of the control test after controlling time of 1 s which is considered as the steady state. The output feedback controller achieves shorter rise time (Reaching 95% of the target deformation, the average rise time in Table III is calculated by averaging the rise time of the three control tests) and better follows the reference value as proven by

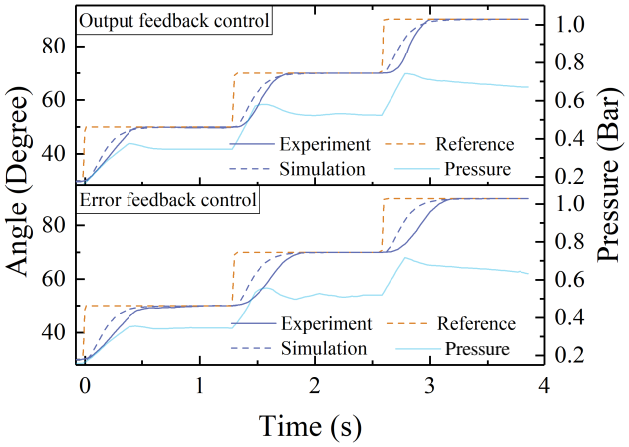

Fig. 8: Example of closed loop shape control of a soft actuator.

TABLE III: Control results

Controller	Error feedback	Output feedback
Average rise time	0.53 s	0.40 s
Static error	$\leq 0.28\%$	$\leq 0.67\%$
RMSE	8.3378	7.393

the RMSE value between the measured angle value and the reference value for the whole control period including three control examples.

III. CONCLUSIONS

This article reports a 3D printed soft actuator that is contactlessly monitored with a cheap webcamera and precisely controlled by an output feedback PID controller with lowpass filter. Some key dimensions that configure the shape of the soft actuator were studied and their influences on the final deformation were simulated using FEM methods. Accordingly, a group of dimension values that offer the maximum deformation and minimum fabrication time was selected for further study. A desktop FDM 3D printer was used for the fabrication which reduced the cost of the actuator. The response model of the actuator was then acquired through data fitting and the controller was designed accordingly to minimize the rising time and ensure a stable shape maintenance. The controller was then implemented and numerous experiments proved that the closed loop control of the 3D printed soft actuator can be realized with fast-response and high accuracy. Compared with our previous study that used error feedback PI controller for the closed loop control, the output feedback controller achieves quicker deformation without violating the control requirements. As a conclusion, this study demonstrates a low cost and feasible method of fabrication and closed loop control of a soft actuator.

During experiments, it was found that after the soft actuator is controlled to the reference shape and the input pressure is stabilized, there is still some slight high frequency position vibrations of the actuator which could result from unstable pressure input, image processing errors or elasticity of the material. These vibration-induced signals are filtered during experiments. However, such signals can lead to the unstable force output of the soft actuator and thus will be studied in the future.

Image feedback provides contactless position sensing but is restricted for one soft actuator monitoring. Grippers composed of multiple actuators as shown in Fig. 1 will pose great challenge for such sensing technology considering the intersection of different actuators. Bending sensors can be used as an alternative if more actuators are required to function cooperatively. Furthermore, The webcamera used in the study provides a maximum frame rate of 30 fps which restricts the sampling time of the total system to be larger than $1/30\ second \approx 33\ ms$. The analysis of images and other calculations and communications also requires time and makes the sampling time of the real time shape control even longer. To make the control process more accurate and stable, the sampling time requires to be reduced in the future. High speed camera and microcontroller boards with more powerful computing power can be used.

ACKNOWLEDGMENT

We appreciate Chun Zhao from Computer School, Beijing Information Science and Technology University for his help on building the closed loop control setup.

REFERENCES

[1] T. Wallin, J. Pikul, and R. Shepherd, "3d printing of soft robotic systems," *Nature Reviews Materials*, vol. 3, no. 6, p. 84, 2018.

[2] M. Schaffner, J. A. Faber, L. Pianegonda, P. A. Rühs, F. Coulter, and A. R. Studart, "3d printing of robotic soft actuators with programmable bioinspired architectures," *Nature communications*, vol. 9, no. 1, pp. 1–9, 2018.

[3] A. Zolfagharian, A. Z. Kouzani, S. Y. Khoo, A. A. A. Moghadam, I. Gibson, and A. Kaynak, "Evolution of 3d printed soft actuators," *Sensors and Actuators A: Physical*, vol. 250, pp. 258–272, 2016.

[4] H. K. Yap, H. Y. Ng, and C.-H. Yeow, "High-force soft printable pneumatics for soft robotic applications," *Soft Robotics*, vol. 3, no. 3, pp. 144–158, 2016.

[5] S. Jiang, F. Liu, A. Lerch, L. Ionov, and S. Agarwal, "Unusual and superfast temperature-triggered actuators," *Advanced materials*, vol. 27, no. 33, pp. 4865–4870, 2015.

[6] K. Kaneto, "Research trends of soft actuators based on electroactive polymers and conducting polymers," in *Journal of physics: conference series*, vol. 704, no. 1. IOP Publishing, 2016, p. 012004.

[7] M. Wang, B.-P. Lin, and H. Yang, "A plant tendril mimic soft actuator with phototunable bending and chiral twisting motion modes," *Nature communications*, vol. 7, no. 1, pp. 1–8, 2016.

[8] A. Zolfagharian, A. Z. Kouzani, S. Y. Khoo, B. Nasri-Nasrabadi, and A. Kaynak, "Development and analysis of a 3d printed hydrogel soft actuator," *Sensors and Actuators A: Physical*, vol. 265, pp. 94–101, 2017.

[9] Y. Kim, H. Yuk, R. Zhao, S. A. Chester, and X. Zhao, "Printing ferromagnetic domains for untethered fast-transforming soft materials," *Nature*, vol. 558, no. 7709, pp. 274–279, 2018.

[10] R. F. Shepherd, F. Ilievski, W. Choi, S. A. Morin, A. A. Stokes, A. D. Mazzeo, X. Chen, M. Wang, and G. M. Whitesides, "Multigait soft robot," *Proceedings of the national academy of sciences*, vol. 108, no. 51, pp. 20 400–20 403, 2011.

[11] P. Kerdlapee, A. Wisitsoraat, D. Phokaratkul, K. Leksakul, R. Phatthanakun, and A. Tuantranont, "Fabrication of electrostatic mems microactuator based on x-ray lithography with pb-based x-ray mask and dry-film-transfer-to-pcb process," *Microsystem technologies*, vol. 20, no. 1, pp. 127–135, 2014.
[12] A. S. Gladman, E. A. Matsumoto, R. G. Nuzzo, L. Mahadevan, and J. A. Lewis, "Biomimetic 4d printing," *Nature materials*, vol. 15, no. 4, pp. 413–418, 2016.
[13] D. K. Patel, A. H. Sakhaei, M. Layani, B. Zhang, Q. Ge, and S. Magdassi, "Highly stretchable and uv curable elastomers for digital light processing based 3d printing," *Advanced Materials*, vol. 29, no. 15, p. 1606000, 2017.
[14] S. Tibbits, "4d printing: multi-material shape change," *Architectural Design*, vol. 84, no. 1, pp. 116–121, 2014.
[15] N. A. Meisel, A. M. Elliott, and C. B. Williams, "A procedure for creating actuated joints via embedding shape memory alloys in polyjet 3d printing," *Journal of intelligent material systems and structures*, vol. 26, no. 12, pp. 1498–1512, 2015.
[16] C. Della Santina, R. K. Katzschmann, A. Biechi, and D. Rus, "Dynamic control of soft robots interacting with the environment," in *2018 IEEE International Conference on Soft Robotics (RoboSoft)*. IEEE, 2018, pp. 46–53.
[17] A. Bajo and N. Simaan, "Hybrid motion/force control of multi-backbone continuum robots," *The International journal of robotics research*, vol. 35, no. 4, pp. 422–434, 2016.
[18] A. Zolfagharian, A. Kaynak, and A. Kouzani, "Closed-loop 4d-printed soft robots," *Materials & Design*, p. 108411, 2019.
[19] T. George Thuruthel, Y. Ansari, E. Falotico, and C. Laschi, "Control strategies for soft robotic manipulators: A survey," *Soft robotics*, vol. 5, no. 2, pp. 149–163, 2018.
[20] K. C. Galloway, K. P. Becker, B. Phillips, J. Kirby, S. Licht, D. Tchernov, R. J. Wood, and D. F. Gruber, "Soft robotic grippers for biological sampling on deep reefs," *Soft robotics*, vol. 3, no. 1, pp. 23–33, 2016.
[21] B. Mosadegh, P. Polygerinos, C. Keplinger, S. Wennstedt, R. F. Shepherd, U. Gupta, J. Shim, K. Bertoldi, C. J. Walsh, and G. M. Whitesides, "Pneumatic networks for soft robotics that actuate rapidly," *Advanced functional materials*, vol. 24, no. 15, pp. 2163–2170, 2014.
[22] X. Zhang, "3d printed soft robot gripper with closed-loop control," Master's thesis, KTH, Mechatronics, 2019.
[23] B. Wittenmark, K. J. Åström, and K.-E. Årzén, "Computer control: An overview," *IFAC Professional Brief*, vol. 1, p. 2, 2002.